3D Flow and Heat Transfer from an Immersed Vertical Cylinder with the Slow Rotation in a Viscous Fluid

Mansourian, Amir[*+]; *B. Rahimi, Asghar*[*+]

Faculty of Engineering, Ferdowsi University of Mashhad, Mashhad, I.R. IRAN

ABSTRACT: *The current study mainly aims to determine the flow and heat transfer from a circular vertical cylinder's slow rotation concerning different viscous fluids bounded by a concentric vertical cylinder. The governing equations are simplified to investigate the possibility of a precise solution. Two sets of partial differential equations with nonlinear coefficients are finally obtained, which are solved using a numerical method to reach a quick result. The impacts of aspect ratio, Prandtl number (Pr), and Richardson number (Ri) are examined on the performance of fluid flow and heat transfer. The bounding cylinder's diameter and height vary from double to quadruple of the rotating cylinder, while the Pr ranges from 55 to 5050. The Ri also varies from 0.01 to 10. The influence of flow decreases near the boundaries as the outer diameter of the boundary increases; the average Nusselt number (Nu) decreases similarly. A change in the Ri from 0.01 to 1 led to the dominance of the forced convection. At mixed convection equal to one and above, natural convection dominates. Small Ri creates vortices in the domain, which disappear by enhancing Ri. The average Nu decreases by changing the Pr number from 55 to 5050. Results are presented as the streamline, isotherms contours, and local as well as average Nu. The details of numerical investigations are compared with the literature which shows a reliable agreement.*

KEYWORDS*: Exact solution; Numerical result; Low-speed rotation; Mix and natural convection; Immersed vertical cylinder.*

INTRODUCTION

The flow between a circular cylinder and its inner shaft has been of interest since the work of Couette in the nineteenth century. Numerous engineering systems such as rotary fractionation columns and electrochemical reactors using rotating cylinder electrodes are required to properly understand the flow field and heat transfer between two coaxial cylinders during the inner cylinder's rotation. One of the considerably important problems is buoyancy-driven flow and heat transfer between a cylinder and the medium around it, extensively applied to different fields such as energy storage tools and crude oil containers. Numerous experimental as well as numerical

studies have addressed this subject.

The first efforts to understand the flow and heat transfer from a rotating vertical cylinder were made to simplify the governing equations and obtain analytical solutions. Many attempts were made in this field until *Nutta* [1] reported an exact solution for torque determination to ensure a circular cylinder's steady rotation within a concentric cylinder-bounded viscous fluid. He simplified the continuity and momentum equation for slow-speed rotational cylinders. *Ostrach* studied natural convection in circular enclosures with no inner objects [2]. He further explored other geometric configurations as well [3–5]. The impact of immersed objects on natural convection in enclosures is another interesting area, including heat transfer in the annulus of concentric horizontal circular cylinders [6] or the natural convections in inner circular objects and outer rectangular enclosures in concentric annulus [7]. Numerical methods created a new branch in research and studies, and most of the results were obtained and presented based on this method, although experimental methods were still used. Several numerical [8–13] and experimental [14–16] studies have investigated natural convection in rectangular enclosures with various aspect ratios, eccentricities, and cross-sections. The rotation of the internal object inside the chamber is also one of the considered issues. *Gupta* and *Goyal* [17] explored incompressible viscous flow between two coaxial rotating circulars with a small uniform injection into the inner cylinder to find a similar solution. *Smith* [18] extended Jeffry's calculations to show more generality of finite vorticity conclusion and then indicated a resolution for the apparent paradox. *Hayase et al.* [19] performed a detailed numerical examination to calculate convective heat transfer between rotating coaxial cylinders in which cavities were embedded periodically and highlighted that in Reynolds number (Re) superficial values, 3D calculations revealed span-wise-dependent Taylor vortex flows in the annulus. However, results showed greater impacts on the flow and heat transfer by locating the cavities on the inner instead of the outer cylinder. *Kimura et al.* [20] experimentally investigated the impacts of the inner rotating plates having a horizontal axis on the heat transfer in differentially heated vertical enclosures. Their result showed the great dependence of the enclosure's heat transfer rate on the Rayleigh number (Ra), defined by 3 regions. The enclosure's heat transfer rate with

the rotating plate showed somehow higher values compared to the rotating cylinder in the forced convection area. Developing numerical methods and optimization of solutions opened a new path in studies. *Ding et al* [21] performed the numerical examination of free convective flows in a horizontal eccentric annulus between square and heated circular outer and inner cylinders, respectively, utilizing a local Multiquadric-Based Differential Quadrature (MQ-DQ) methodology. As shown by their results, the proposed method could provide accurate simulations of the natural convection problem under a large Ra (106). *King* and *Wilson* [22] conducted a numerical simulation of convection heat transfer in Rayleigh-Benard Convection (RBC) and rotating annulus, indicating the Nu and Ra (Nu~RaɣY) correlation, in which the Ɣ was equal to 1/3. *Keh* and *Wang* [23] examined a circular cylinder's motion undergoing slip nearby the plane wall and indicated a reduction in the boundary-corrected drag force and torque that acted on the particle with increased slip coefficient for otherwise determined conditions. A cylinder led to more significant hydrodynamic drag force and torque enhancement on a particle that translates and rotates due to a neighboring plane wall compared to a sphere.

Paramane and *Sharma* [24] studied heat and fluid flow over rotating circular cylinders in the laminar state for Re range of 20-160 and constant Pr (Pr=0.7). A downward lift force was observed because of rotation with a monotonic increase by increasing non-dimensional rotation rate and remained almost constant with enhancing Re. The average Nu showed a decrease and increment as the rotation rate and Re number increased, respectively, becoming nearly constant at the maximum rotation rates at all levels of Re. *Baradaran Rahimi* and *Jabari Moghadam* [25] developed a similar solution for the flow and heat transfer examination between two rotating spheres which had constant angular velocities. *Costa* and *Raimundo* [26] investigated steady mixed convection in differentially heated square enclosures that had active rotating circular cylinders. To better understand the cylinder's contribution to heat transfer, the authors examined the local heat exchange across the surface of the cylinder and the fluid. The rotating cylinder's impacts on the enclosure's thermal performance were highlighted, confirming the critical role of the cylinder's thermophysical characteristics in the entire process of heat transfer along the enclosure. *Hussain* and

Hussain [27] focused on the impacts of vertical cylinder locations and Ra on fluid flow and performance of heat transfer, revealing an increase in the average and local Nu with various locations upwards and downwards the inner cylinder as the Ra increases, which could be associated with considerable impacts of thermal convection. However, there was a thin thermal boundary layer under higher Ra values as the flow actively reached the square enclosure's uppermost and bottommost. *Silva et al.* [28] conducted a numerical simulation of flows in rotating circular cylinders utilizing the immersed boundary methodology. Different values of Re (60, 100, and 200) and specific rotations were considered for simulations. Evaluation of the rotation impacts on the characteristics of the flow and fluctuating forces was conducted while reducing convergence time and increasing the precision of the problem-solving. *Liao and Lin* [29] employed an immersed-boundary methodology for the natural and forced convection simulation in a complex geometry domain considering low Re values. They indicated the impacts of the solid-body-forcing and the implementation of the isothermal and iso flux boundary conditions, declaring that the thermal field solid-body-forcing was unnecessary due to its insignificant impacts on the thermal and dynamic field with the stationary embedded objects in the velocity range under study. *Liao and Lin* [30] focused on the mixed convection of heated rotating cylinders in square enclosures investigating the aspect ratio, Ra, and Pr impacts on heat transfer. The authors confirmed the independence of the average Nusselt and Rayleigh for Ri<1, with the average Nusselt decreasing as the aspect ratio increased. *Usman Ikhtiar et al.* [31] examined free stream flows and forced convection heat transfer throughout rotating circular cylinders under single gust impulses indicating more sensitivity of the flow physics and heat transfer features to the upstream gust at greater rotation rates. Besides, the temperature characteristics and the variation in the Strouhal number maximum in the second vortex shedding regime were addressed. As shown by the authors, the upstream gust resulted in increased average Nu in the 1st and 2nd vortex shedding states. *Hanif et al.* [32] studied the gust impulse impacts on the transient flows and forced convection heat transfer within rotating circular cylinders near plane boundaries focusing on a 2D and incompressible flow regime. According to their findings, an increase in the circular cylinder rotation rates in the 2nd vortex shedding state resulted in the separation

as well as a rollover in the plane wall boundary layer even for the greater ratios of gap-to-diameter. However, just impulses in these systems led to significant alterations in immediate Nu distribution over the cylinder circumference. *Deepak Kumar et al.* [33] studied the motion of Powell-Eyring fluid between two concentric rotating cylinders and proposed a solution for the governing equations utilizing Schauder's fixed point theorem. As shown by the authors, the velocity was an increasing function of the rotation and Powell-Eyring fluid parameters. *M. Hatami et al.* [34] used a numerical solution to investigate the rotating cylinder turbulator effect on the heat transfer of a nanofluid flow in a wavy divergent channel. They assumed that rotating cylinder makes vortexes to increase heat transfers. They tried to indicate the effect of nanoparticle volume fraction, Reynolds number, cylinder diameter, and rotating velocity. Their results show that increasing the Re number has the most effect on heat transfer. *Somayeh Davoodabadi* and *Hakan F. Oztop* [35] investigated the effect of changes in the width of the cavity, the radius of the rotational and vibrational cylinder, and the effect of the rotational speed on natural convection in a rectangular tall cavity. They assumed the vibration of the cylinder in the Y-direction and a sinusoidal form. Their result shows that as the angular velocity, vibration amplitude, and frequency increase, the heat transfer rate increases.

So far, the analytical solution of the 3D energy equation for a submerged vertical rotating cylinder at low speed has not been studied and the effect of geometrical parameters, and fluid type has not been reported. In this manuscript, it has tried to investigate these cases, and report the results.

THEORETICAL SECTION
Physical modeling
Geometry and equation

Fig. 1 depicts the 3D configuration of a rotating vertical cylinder with different geometry (radius and heights). The vertical cylinder and the chamber are concentric; where and b show the inner and outer radius of vertical cylinders, respectively. S_I and S_o also show half-height of cylinders.

Moreover, *w* is rotational speed, and *r* and *z* represent the cylindrical coordinate systems. The symbol I denotes the upper and lower regions of the inner cylinder, while the annular region is marked by Π.
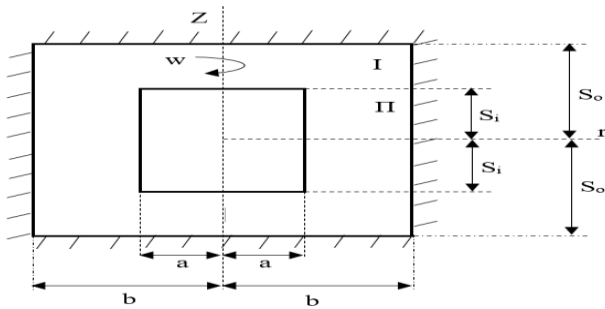
Assuming a steady and incompressible flow in cylindrical

Fig. 1: Geometry and defined geometrical parameters

coordinates, it is possible to write the governing relations as [36]:

Continuity Eq:

$$\frac{1}{\rho}\frac{\partial \rho}{\partial t} + \frac{1}{r}\frac{\partial}{\partial r}(rv_r) + \frac{1}{r}\frac{\partial v_\theta}{\partial \theta} + \frac{\partial v_z}{\partial z} = 0 \tag{1}$$

Momentum Eq:

r direction:

$$\frac{\partial v_r}{\partial t} + (v,\nabla)v_r - \frac{1}{r}v_\theta{}^2 = -\frac{1}{\rho}\frac{\partial p}{\partial r} + g_r$$

$$+\vartheta(\nabla^2 v_r - \frac{v_r{}^2}{r^2} - \frac{2}{r^2}\frac{\partial v_\theta}{\partial \theta}) \tag{2}$$

θ direction:

$$\frac{\partial v_\theta}{\partial t} + (v.\nabla)v_\theta - \frac{1}{r}v_r v_\theta = -\frac{1}{\rho r}\frac{\partial p}{\partial \theta}$$

$$+g_\theta + \vartheta(\nabla^2 v_\theta - \frac{v_\theta}{r^2} + \frac{2}{r^2}\frac{\partial v_r}{\partial \theta}) \tag{3}$$

z direction:

$$\frac{\partial v_z}{\partial t} + (v.\nabla)v_z = -\frac{1}{\rho}\frac{\partial p}{\partial z} + g_z +$$

$$\nabla^2 v_z - g\beta(T - T_c) \tag{4}$$

Energy Eq:

$$\rho C_p \left[\frac{\partial T}{\partial t} + (v.\nabla)T\right] = k\nabla^2 T + \mu\varphi \tag{5}$$

Here φ is the dissipation term that:

$$\varphi = 2(\epsilon_{rr}{}^2 + \epsilon_{\theta\theta}{}^2 + \epsilon_{zz}{}^2) +$$

$$\epsilon_{rz}{}^2 + \epsilon_{\theta z}{}^2 + \epsilon_{r\theta}{}^2 \tag{6}$$

$$\epsilon_{rr} = \frac{\partial v_r}{\partial r} \qquad \epsilon_{rz} = \frac{\partial v_r}{\partial z} + \frac{\partial v_z}{\partial r}$$

$$\epsilon_{\theta\theta} = \frac{1}{r}\left(\frac{\partial v_\theta}{\partial \theta} + v_r\right) \qquad \epsilon_{rz} = \frac{1}{r}\left(\frac{\partial v_r}{\partial \theta} + v_\theta\right) + \frac{\partial v_\theta}{\partial r}$$

$$\epsilon_{zz} = \frac{\partial v_z}{\partial z} \qquad \epsilon_{rz} = \frac{\partial v_\theta}{\partial z} + \frac{1}{r}\frac{\partial v_z}{\partial \theta}$$

Regarding the symmetry of the domain in the θ direction, zero velocity in r direction, negligible dynamic and static pressures due to the low velocity, nominal length of the vertical cylinder, and zero nonlinear terms because of low speed, the governing equation can be rewritten as:

$$\frac{\partial v_z}{\partial z} = 0 \to v_z = f(r) \text{ although we know } v_\theta = f(r,z)$$

$$\begin{cases} (v.\nabla)v_\theta = \vartheta\left(\nabla^2 v_\theta - \frac{v_\theta}{r^2}\right) \\ (v.\nabla)v_z = \vartheta\nabla^2 v_z - g\beta(T - T_c) \end{cases} \tag{7}$$

$$\rho C_p(v.\nabla)T = k\nabla^2 T$$

The boundary condition of the system is as follows:

$$\text{Domain of I}: \begin{cases} z=S_i \begin{cases} 0<r<a \begin{cases} V_\theta = a*w \\ V_z = 0 \\ T = T_H \end{cases} \\ a<r<b \begin{cases} V_\theta|_I = V_\theta|_{II} = r*w \\ \frac{\partial V_z}{\partial z}\big|_I = \frac{\partial V_z}{\partial z}\big|_{II}, V_z|_I = V_z|_{II} \\ \frac{\partial V_\theta}{\partial z}\big|_I = \frac{\partial V_\theta}{\partial z}\big|_{II}, \theta|_I = \theta|_{II} \end{cases} \end{cases} \\ z=S_o, 0\leq r\leq b \begin{cases} V_\theta = 0 \\ V_z = 0 \\ T = T_C \end{cases} \end{cases} \tag{8}$$

$$\text{Domain of II}: \begin{cases} z = 0, a < r < b \begin{cases} V_\theta = a*r \\ \frac{\partial V_z}{\partial z} = 0 \\ \frac{\partial V_\theta}{\partial z} = 0 \end{cases} \\ r = b, 0 < z \leq S_i \begin{cases} V_\theta = 0 \\ V_z = 0 \\ T = T_C \end{cases} \\ r = a, 0 < z \leq S_i \begin{cases} V_\theta = a*w \\ V_z = 0 \\ T = T_H \end{cases} \end{cases} \tag{9}$$

Now the dimensionless parameters define as follows:

$$X = \frac{r}{a} \qquad Y = \frac{z}{a}$$

$$\lambda = \frac{b}{a} \qquad U_0 = a.w \tag{10}$$

$$\theta^{\cdot\cdot} = \frac{T - T_c}{T_H - T_c} \qquad V_r = \frac{v_r}{U_0}$$

$$V_z = \frac{v_z}{U_0} \qquad V_\theta = \frac{v_\theta}{U_0}$$

Where, a and b represent the inner and outer vertical cylinder radii, respectively. u_r, u_z, u_θ show the respective components of velocity in the r,z,s and θ directions, while U_0 indicates the reference velocity. T_H, and T_c show the inner and outer vertical cylinder temperatures, respectively. In cylindrical coordinates, the divergence $(V.\nabla)$ and ∇^2 operators are defined as follows:

$$V.\nabla = v_r\frac{\partial}{\partial r} + \frac{1}{r}v_\theta\frac{\partial}{\partial \theta} + v_z\frac{\partial}{\partial z} \tag{11}$$

$$\nabla^2 = \frac{1}{r}\frac{\partial}{\partial r}\left(r\frac{\partial}{\partial r}\right) + \frac{1}{r^2}\frac{\partial^2}{\partial \theta^2} + \frac{\partial^2}{\partial z^2}$$

With the substitute from (10):

$$V.\nabla = \frac{U_0 V_r}{a}\frac{\partial}{\partial X} + \frac{U_0}{aX}V_\theta\frac{\partial}{\partial\theta} + \frac{U_0}{a}V_y\frac{\partial}{\partial Y} \rightarrow \quad (12)$$

$$V.\nabla = \frac{U_0}{a}(V.\nabla^{..})$$

$$\nabla^2 = \frac{1}{aX}\frac{1}{a}\frac{\partial}{\partial X}\left(aX\frac{1}{a}\frac{\partial}{\partial X}\right) + \frac{1}{a^2 X^2}\frac{\partial^2}{\partial\theta^2} + \frac{1}{a^2}\frac{\partial^2}{\partial Y^2} \rightarrow$$

$$= \frac{1}{a^2}\nabla^{..2} = \frac{1}{a^2}\{\frac{1}{X}\frac{\partial}{\partial X}\left(X\frac{\partial}{\partial X}\right) + \frac{1}{X^2}\frac{\partial^2}{\partial\theta^2} + \frac{\partial^2}{\partial Y^2}\}$$

According to Eq. (12), mentioned assumptions, and the Boussinesq approximation, the dimensionless equations can be expressed by:

b.2 equation (Momentum at the θ directin):

$$\frac{U_0^2}{a}(V.\nabla^{..})V_\theta = \nu(\frac{U_0}{a^2}\nabla^{..2}V_\theta - \frac{U_0}{a^2}\frac{V_\theta}{X^2}) \rightarrow$$

$$(V.\nabla^{..})V_\theta = \frac{\nu}{aU_0}\left(\nabla^{..2}V_\theta - \frac{V_\theta}{X^2}\right) = \frac{1}{Re}\left(\nabla^{..2}V_\theta - \frac{V_\theta}{X^2}\right) \quad (13)$$

b.3 equation (Momentum at the z direction):

$$\frac{U_0^2}{a}(V.\nabla^{..})V_Y = \nu\frac{U_0}{a^2}\nabla^{..2}V_Y - g\beta(T - T_c)$$

$$\times\frac{(T_h - T_c)}{(T_h - T_c)}\times\frac{a^2}{a^2}\times\frac{\nu^2}{\nu^2} \rightarrow$$

$$(V.\nabla^{..})V_Y = \frac{\nu}{aU_0}\nabla^{..2}V_Y - \frac{g\beta(T_h - T_c)a^3}{\nu^2}\times\frac{\nu^2}{a^2 U_0}\theta^{..} \rightarrow$$

$$(V.\nabla^{..})V_Y = \frac{1}{Re}\nabla^{..2}V_Y - \frac{Gr}{Re^2}\theta^{..} \quad (14)$$

c equation (energy equation):

Since T_c is constant and we want to take the derivative of T, we can write $T - T_c$ instead:

$$\rho C_p\left[\frac{\partial\{(T-T_c)\times\frac{(T_h-T_c)}{(T_h-T_c)}\}}{\partial t} + (V.\nabla)\{(T-T_c)\times\frac{(T_h-T_c)}{(T_h-T_c)}\}\right] =$$

$$K\nabla^2\{(T - T_c)\times\frac{(T_h-T_c)}{(T_h-T_c)}\}$$

$$\rho C_p\left[\frac{U_0}{a}\times(T_h - T_c)(V.\nabla^{..})\theta^{..}\right] = \frac{K(T_h-T_c)}{a^2}\nabla^{..2}\theta^{..}$$

$$(V.\nabla^{..})\theta^{..} = \frac{K}{aU_0\rho C_p}\times\frac{\mu}{\mu}\nabla^{..2}\theta^{..} \quad (15)$$

$$(V.\nabla^{..})\theta^{..} = \frac{1}{Pr\,Re}\nabla^{..2}\theta^{..}$$

So, we have system of equations:

$$\begin{cases}(V.\nabla^{..})V_\theta = \frac{1}{Re}\left(\nabla^{..2}V_\theta - \frac{V_\theta}{X^2}\right)\\(V.\nabla^{..})V_Y = \frac{1}{Re}\nabla^{..2}V_Y - Ri\theta^{..}\\(V.\nabla^{..})\theta^{..} = \frac{1}{Pr\,Re}\nabla^{..2}\theta^{..}\end{cases} \quad (16)$$

The dimensionless characterizing parameters are the Ri, defined as $Ri = \frac{Gr}{Re^2}$ where Gr is the Grashof number ($Gr = \frac{g\beta(T_H - T_c).a^3}{\nu^2}$ in which β is the thermal expansion coefficient, g is the gravitational acceleration, and ν Kinematic viscosity of the fluid), $Re = \frac{a.U_0}{\nu}$ (the rotation Re), and $= \frac{\nu}{\alpha}$. There is an insignificant thermal radiation related to heat transfer among the walls, and the fluid has been considered non-participating from the radioactive perspective. The energy terms associated with viscous dissipation and temperature variations because of reversible deformation (work of pressure forces) have not been considered [30]. Also, the boundary conditions in the dimensionless state change as follows:

Domain of I :

$$\begin{cases}Y = Y_i\begin{cases}0 < X < 1\begin{cases}V_\theta = X\\V_Y = 0\\\theta^{..} = 1\end{cases}\\1 < r < \lambda\begin{cases}V_\theta|_I = V_\theta|_\Pi = X\\\frac{\partial V_Y}{\partial Y}\Big|_I = \frac{\partial V_Y}{\partial Y}\Big|_\Pi, V_Y|_I = V_Y|_\Pi\\\frac{\partial V_\theta}{\partial Y}\Big|_I = \frac{\partial V_\theta}{\partial Y}\Big|_\Pi, \theta^{..}|_I = \theta^{..}|_\Pi\end{cases}\end{cases}\\Y = Y_o, 0 \le X \le \lambda\begin{cases}V_\theta = 0\\V_Y = 0\\\theta^{..} = 0\end{cases}\end{cases} \quad (17)$$

Domain of Π:
$$\begin{cases}Y = 0, 1 < X < \lambda\begin{cases}V_\theta = X\\\frac{\partial V_Y}{\partial Y} = 0\\\frac{\partial V_\theta}{\partial Y} = 0\end{cases}\\X = \lambda, 0 < Y \le Y_i\begin{cases}V_\theta = 0\\V_Y = 0\\\theta^{..} = 0\end{cases}\\X = 1, 0 < Y \le Y_i\begin{cases}V_\theta = 1\\V_Y = 0\\\theta^{..} = 1\end{cases}\end{cases}$$

The chamber walls were considered perfectly isotherm. Because of the surface velocity non-slip boundary conditions, a forced flow results from the vertical cylinder (with the radius a) rotation, leading to a mixed convection. The wall effects on the heat transfer process were examined by changing the chamber geometry. Three various types of fluid were used to fill the free space in the enclosure. The pressure changes (incompressible fluid) did not affect the fluid, but temperature affected it. Density in the buoyancy term depended on temperature, leading to the use of Boussinesq approximation.
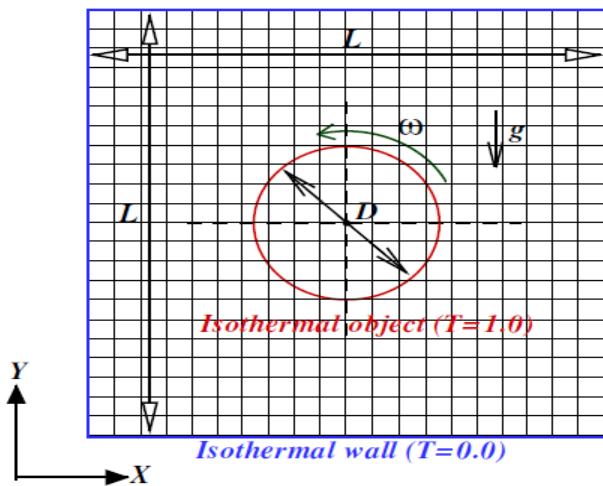
Independence of mesh

One of the most critical and influential parameters of numerical simulation, which is effective in simulation cost and time, meshes independence. The ICEM 19.1 software

Table 1: comparison of average Nusselt number at the surface of vertical rotational cylinder, for different grids

Mesh	425110	593128	725182	970361
Average Nusselt number	13.011	13.841	14.528	14.943
Error (%)	12.9	7.4	2.8	-

Table2: comparison of local Nusselt number at the surface of inner circle, between present work and results in reference

Surface of inner circle at the different degree	Local Nusselt number		
	Present study	Chuan-Chieh Liao, Chao-An Lin [29]	Error(%)
0	6.943	6.93	0.2
45	6.534	6.8	4.1
90	5.706	5.9	3.4
135	5.178	5.5	6.2
180	5.564	5.6	0.6
225	6.183	5.8	6.2
270	7.001	6.8	2.9
315	7.441	7.35	1.2
360	6.94	6.93	0.2

Fig. 2: Computational domain and boundary conditions for mixed convection in the annulus between concentric rotating circular cylinder and square enclosure

was used for the structure and non-structured hexagonal cells. To increase the accuracy and reduce the solution time near the boundary of the rotating vertical cylinder, the boundary layer mesh has been used. Four grid numbers (425110, 593128, 725182, and 970361) were utilized to calculate the average Nusselt number on a vertical rotational cylinder in Ri=1, Pr=12.5, and b/a=2. Based on the obtained results in table 1, the best choice is related to the selection of 725182 meshes.

Validation of results

To validate mix convection models, the present model was simplified and the obtained local Nu were compared with the reported result from reference [30] whose geometry is depicted in Fig 2. The simulated data were compared with the reports of *Chuan-Chieh Liao, Chao-An Lin* to validate the results as shown in table 2. The numerical results well predicted local Nu with less than 6% difference. The results of this study were showed acceptable consistency with the previously conducted study for the condition with $\frac{L}{D} = 2.5$, $Ri = 10$, and Pr=0.71.

RESULTS AND DISCUSSION

The current section discusses the mixed convection in the space of two concentric vertical cylinders with an active rotating circular vertical cylinder according assumption of steady state flow, viscous incompressible fluid, Laminar flow, no-slip, isothermal boundary Richardson number (Ri) was considered as the dimensionless parameter to examine the corresponding significance of the natural and forced convections ($Ri = \frac{Gr}{Re^2}$, in which Re represents the rotational Re, found by $Re = \frac{a^2.w}{v}$). The influences of three factors of Ri, the aspect ratio $\left(\frac{b}{a}\right)$, and the Pr were assessed on the heat transfer. The effect of the Pr was investigated by considering three different fluids:

engine oil ($Pr = 1205$), ethylene glycol ($Pr = 55$), and oil 47V500($Pr = 5050$).

Influences of the Richardson number

The effect of the rotational vertical cylinder was evaluated on the heat transfer rates for different Ri values and $\frac{b}{a} = 2$ and Pr=1205. The isotherm contour and streamlines are depicted in Fig. 3 for different Ri values (0.01, 0.5, 1, 5, and 10).

The rotational vertical cylinder influenced the flow structures. Two anti-symmetric recirculating vortices were found at midplane XY in Fig. 3(e1) for when Ri=10. With the increase of *w*, a small anti-symmetric circulation formed from the top of the rotational vertical cylinder. With further rise of the rotational speed, the circulation growth increased. For Ri=0.01, four counter-clockwise circulations dominated the flow, caused by the rotating vertical cylinder, as shown in the streamlines of Fig. 3 (a1–e1). Interestingly, four clockwise vortices emerged for Ri=0.01. The convective strength rose by decreasing the Ri=1. For Ri>1, the isotherm contour moved upwards with a plume present on the topmost. The influence of the rotating vertical cylinder on the isotherm contour is similar to the case for streamline.

At Ri=0.01 (high rotation speeds), the flow field was dominated by the forced convection heat transfer. The predominance of forced convection over free convection can be also observed in shape of 3D streamlines and temperature contours. With an increment in Ri, the intensity of forced convection and the effect of free convection showed an increase and decrease, respectively. Concerning streamlines, approximately 50% of the movements were rotational and the remaining 50% were transitional in Ri=1. Ri=1 was the turning point which changed the dominant mechanism of convection heat transfer. Examination of streamlines at Ri=10 showed that almost all heat transfer was free convection and the tendency of vertical motion was much higher than rotational movements.

Fig. 4 indicates the associations of the surface-averaged Nu (Nu_{Mean}) and the Ri. The Nu_{Mean} showed slight variations for Ri>1. The Nu_{Mean} decreased by enhancing Ri. An approximately more dramatic reduction was evident as Ri changed from 0.01 to 0.5. Further enhancement of Ri above 5 led to independence of the predicted Nu_{Mean}

from Ri. Based on Figs. 3(a2, e2), the isotherm spacing near the vertical cylinder increased by elevating Ri, reflecting the thermal boundary layer's thickening and thus the relative decrease in the temperature gradient as well as Nu_{Mean} such that this reduction from Ri=0.01 to Ri=10 was about 85%.

The distribution of local Nu along the hot and cold surfaces of the vertical cylinder are depicted in Fig. 5 considering different values of Ri for b/a=2. A local maximum value is evident near the top wall of the outer vertical cylinder, whereas four minimum values are found on the lower and top walls of the outer vertical cylinder. The differences of the local Max. and Min. Nu (Nu Difference) decreased as Ri went up. At Ri=0.01 (see Fig. 5), the thermal gradient on the middle part of the outer vertical cylinder got stronger, whereas the movements away from the center to upper and lower surfaces was weakened. Unlike the outer vertical cylinder, thermal gradients were stronger on the top and lower walls of the inner vertical cylinder, resulting in high local Nusselt values.

By increasing Ri, the locations of both local minimum and maximum Nu moved along the Y direction. The lower wall of the vertical cylinder showed a stronger thermal gradient by decreasing the rotational speed of the vertical cylinder, leading to maximum Nusselt in this area. With further rise of Ri and predominance of free convection, the fluid moved upward and the thermal gradient decreased along the vertical cylinder's axis; therefore, the Nu reduced as excepted at Y=0.01. This is due to the higher temperature gradient in the area above the wall as a result of higher heat flux transferred from the vertical cylinder's top to the fluid.

Influences of aspect ratio

The rotational vertical cylinder's effect was further explored on the heat transfer rates at various aspect ratios for Pr=1205. The results are presented in Fig. 3 for b/a=2, while the 2D and 3D streamlines and isotherm contour are respectively shown in Figs. 6 and 7 for b/a=3 and 4.

Figs. 3(a2), 6(a2), and 7(a2) show the temperature contour. Fig. 3 indicates a single plume structure at the midplane of the domain. Since the effect of force convection decreases with increasing Ri number, the plume structure disappeared, and the effect of free convection became more evident by the upward shift of the
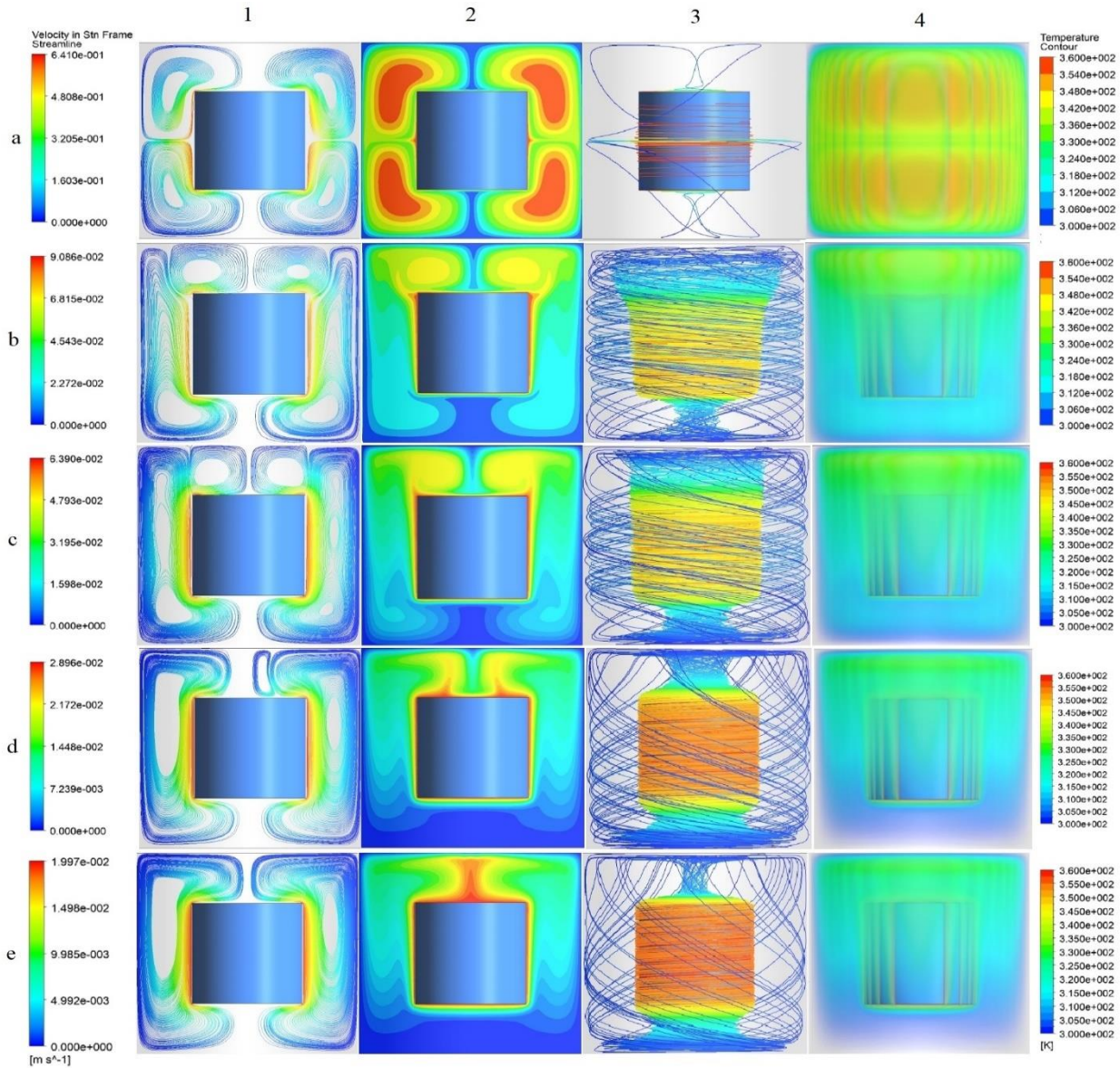
Fig. 3: 2D and 3D streamlines and isotherm contour for different value of Ri at b/a=2 and Pr=1205, a(Ri=0.01), b(Ri=0.5), c(Ri=1), d(Ri=5), e(Ri=10)
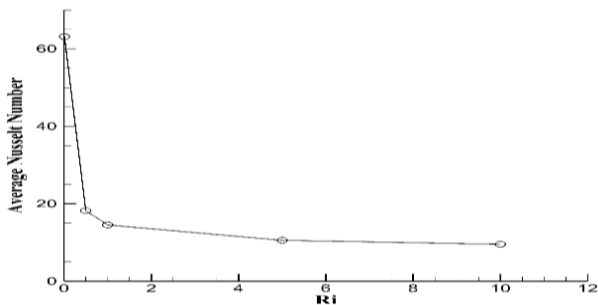

Fig. 4: The relationship between the surface-averaged Nusselt number (Nu_{Mean}) and Richardson number (Ri) when b/a=2 and Pr=1205

isotherm temperature lines. This plume is also evident in the streamlines. For high Ri values, this plume changed. Concerning the aspect ratio, the vortices formed in Ri=0.01 did not disappear with increasing Ri number when the aspect ratio was increased. These vortices also affected heat transfer.

Fig. 8 indicates the association of the surface-averaged Nu (Nu_{Mean}) and Ri in the case of three various aspect ratios with similar distributions, revealing a decrease in the Nu_{Mean} with the increase of Ri. With increasing the Ri,
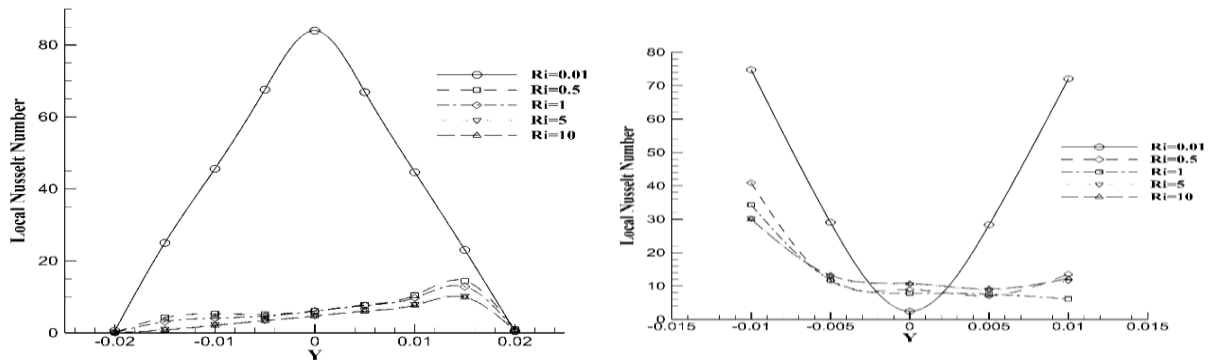
Fig. 5: Comparison of local Nusselt number distribution along the surface: left inner vertical cylinder, right outer enclosure for different values of Y and Ri when Pr=1205 and b/a=2

the thermal boundary layerwas declined, reducing the heat transfer rate, hence a decrement in Nu_{Mean}. By increasing the aspect ratio at the Ri = 0.01, in which the dominant heat transfer is in the form of forced convection, the amount of heat transfer increased, which enhanced the average Nu number.

Fig. 9 depicts the distribution of the local Nu along the inner vertical cylinders for two aspect ratios of 3 and 4. The variation trend was similar to the case with b/a=2. Based on Figs. 5 and 9, except for Ri=0.01, the local Nusselt decreased with increasing Ri. For fixed Ri, however, the local Nusselt decreased with enhancement of the aspect ratio.

Influences of Prandtl Number

This section is devoted to studying the impacts of Pr on the flow and heat transfer considering b/a=2. Fifteen numerical simulations were performed Pr=55, over most of the domain for Pr=5050 and shrank with a decrease in Pr until disappearing for Pr=55. For fixed thermal diffusivity, the viscosity was declined by decrementing Pr. Many vortices were formed in the fluid upon reducing the Pr number which were transported up the domain by increasing the Ri and the Buoyancy effect. By decreasing Pr number, the problem solving got unstable such that less than ten problems became completely unstable and the flow got unsteady in a critical Pr value.

The distribution of local Nu over inner and outer vertical cylinder is shown in Figs. 12 and 13 for Pr=5050 and 55, respectively. The effects of fluid instability on the inner vertical cylinder wall can be seen in local Nusselt variations with decreasing Pr number. In Fig. 13, the forced convection was the dominant heat transfer up to

Ri=1; i.e., the effect of rotational motion on the dominant buoyant motion. Examination of the local Nusselt changes on the outer vertical cylinder indicated that the diagram had a maximum point which moved towards the upper wall with increasing the buoyancy effect and dominance of free convection.

The association of the Nu_{Mean} and Ri is shown in Fig. 14 for different Pr values when b/a= 2. The dynamic and thermal fields' state depended on the rotation strength. As the Pr number decreased, the rotation intensity spread more in the fluid. According to Fig.14, the average Nusselt rate decreased by the decline of the Pr to a constant Ri. In a fixed Pr, as expected, with increasing Ri and the predominance of free-convection heat transfer, the amount of thermal boundary layer decreased, after which a decrement in average heat transfer and average Nu was evident.

The reduction of average Nu at the different Ri and the different Pr values shown in Table 1.

This decreasing trend suggests that the effect of changing Ri from 1 to 5 was higher than its variation from 0.5 to 1 which can be due to the overall effect of the free convection phenomenon.

CONCLUSIONS

A three-dimensional laminar version of the control-volume-based Finite element method (FEM) has been utilized to provide the numerical solution for the flow and heat transfer between rotating coaxial vertical cylinders with an embedded vertical cylinder rotating at a low rotational speed. The method has been first validated with forced convection-induced flows in the annulus between the concentric circular vertical cylinder and square enclosure, then the effect of the low rotation speeds of inner vertical cylinder on the heat transfer phenomena and flow characteristics has been investigated. The effects of
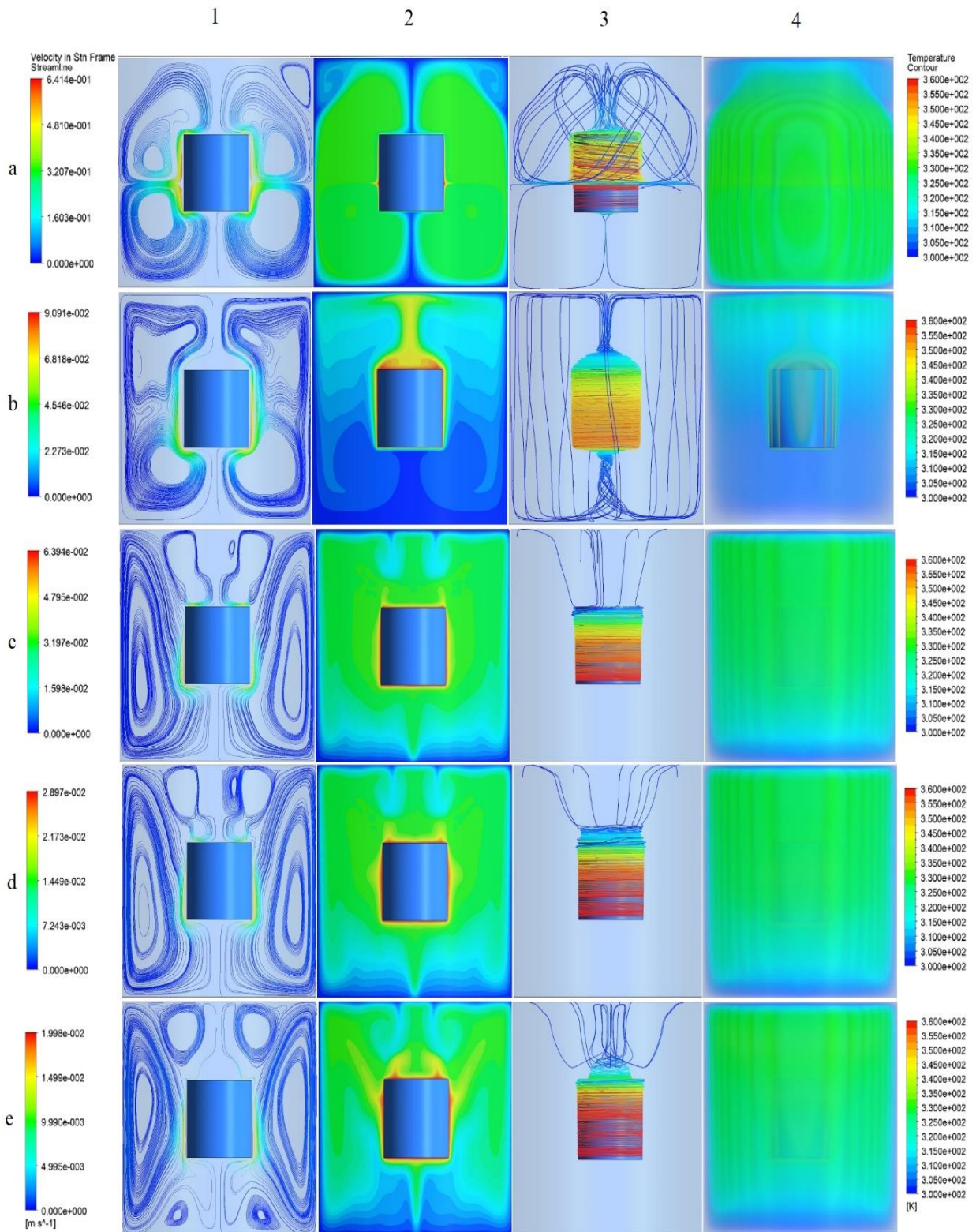
Fig.6: 2D and 3D streamlines and isotherm contour for different value of Ri at b/a=3 and Pr=1205, a(Ri=0.01), b(Ri=0.5), c(Ri=1), d(Ri=5), e(Ri=10)

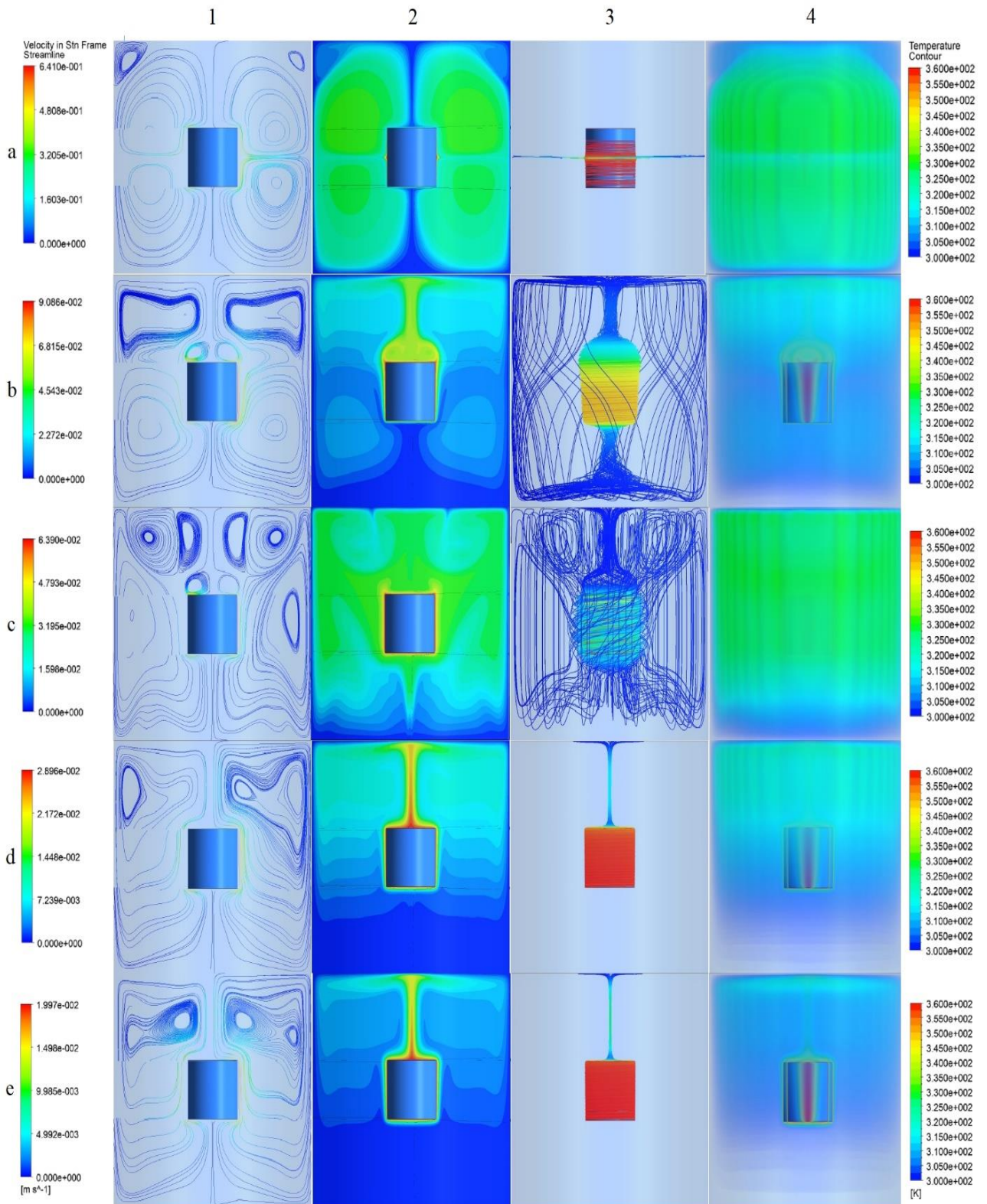*Fig. 7: 2D and 3D streamlines and isotherm contour for different value of Ri at b/a=4 and Pr=1205, a(Ri=0.01), b(Ri=0.5), c(Ri=1), d(Ri=5), e(Ri=10)*
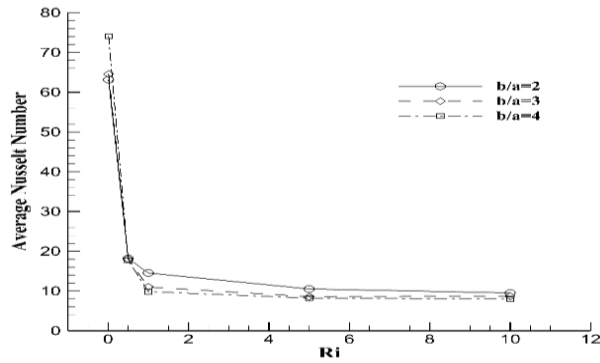
Fig. 8. The relationship between the surface-averaged Nusselt number (NuMean) and Richardson number (Ri) for different aspect ratio (b/a) when Pr =1205
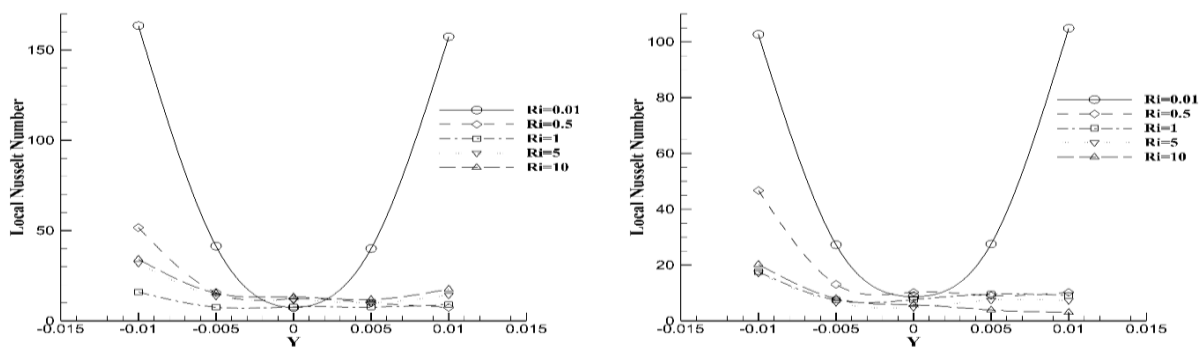

Fig. 9: Comparison of local Nusselt number distribution along the surface of the inner vertical cylinder: left b/a=3, right b/a=4

Richardson Number (Ri), aspect ratio (b/a), and Prandtl number (Pr) have been addressed on the heat transfer. The conclusions below are drawn according to the evidence collected by the current research:

1) Concerning the impacts of Ri, the flow structures have been affected by the rotational vertical cylinder for $\frac{b}{a} = 2$ and Pr=1205. Two anti-symmetric recirculating vortices have been observed at midplane XY for Ri=10. By enhancing $\boldsymbol{w}$, a small anti-symmetric circulation has been formed from the top of the rotational vertical cylinder. For Ri=0.01, the flow has been dominated by the four counter-clockwise circulations induced by the rotating vertical cylinder. By increasing the Ri=1, the convective strength has elevated. For Ri>1, the isotherm contours have moved upward with a plume appearing on the top. When Ri<1, the flow field has been under complete influence of the forced convective heat transfer, while at Ri>1, the free convection has predominated. Ri=1 has been the turning point as it has changed the dominant mechanism of convective heat transfer. The Average Nusselt Number (NuMean) has decreased in tandem with increased Ri, and a

relatively sharper reduction was evident when Ri has altered from 0.01 to 0.5. When the Ri has further decreased to more than five, the predicted NuMean has been independent of Ri. The reduction for average Nusselt from Ri=0.01 to Ri=10 has been close to 85%.

2) The rotational vertical cylinder's impacts on the heat transfer rates have been assessed under various aspect ratios considering Pr=1205. In all aspect ratios, a clear single plume structure has appeared on the domain's mid-plane for Ri=0.01. Since the effect of forced convection has decreased with increasing Ri, the plume structure has disappeared. The effect of this plume has not completely disappeared with elevating the aspect ratio at high Ri values and has remained as small vortices in the fluid. Concerning the aspect ratio impacts, the association of the predicted NuMean and Ri has been similar for three various aspect ratios, indicating a decline in the NuMean with the decrement of Ri. Besides, smaller aspect ratios have generated higher Nu values, revealing improved heat transfer. The decrease in the averaged Nusselt number because of the changing Ri number from 0.01 to 10 has been 84.9%, 86.5%, and 89.2% for b/a=2, 3, and 4, respectively.
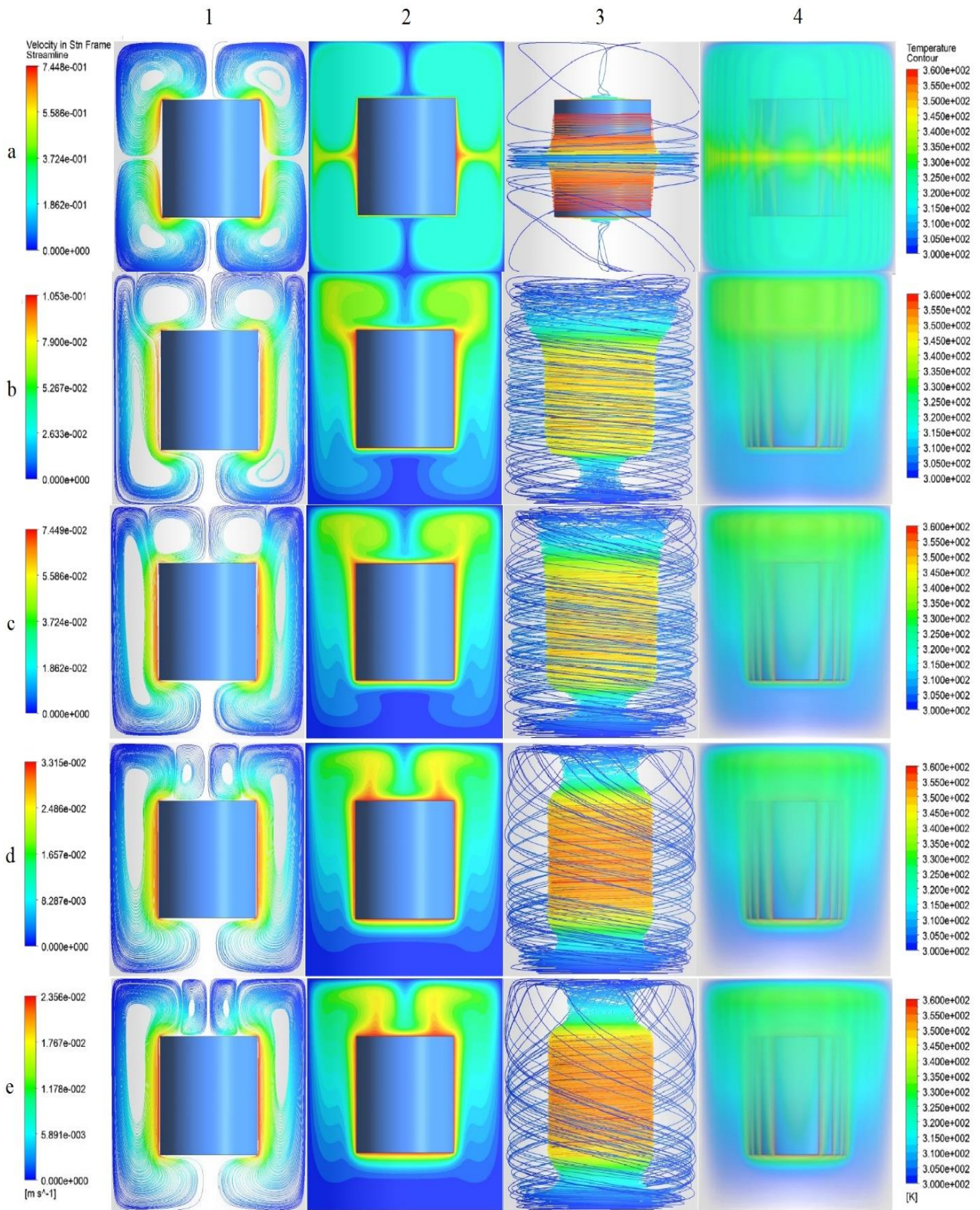
Fig: 10: 2D and 3D streamlines and isotherm contour for different value of Ri at b/a=2 and Pr=5050, a(Ri=0.01), b(Ri=0.5), c(Ri=1), d(Ri=5), e(Ri=10)
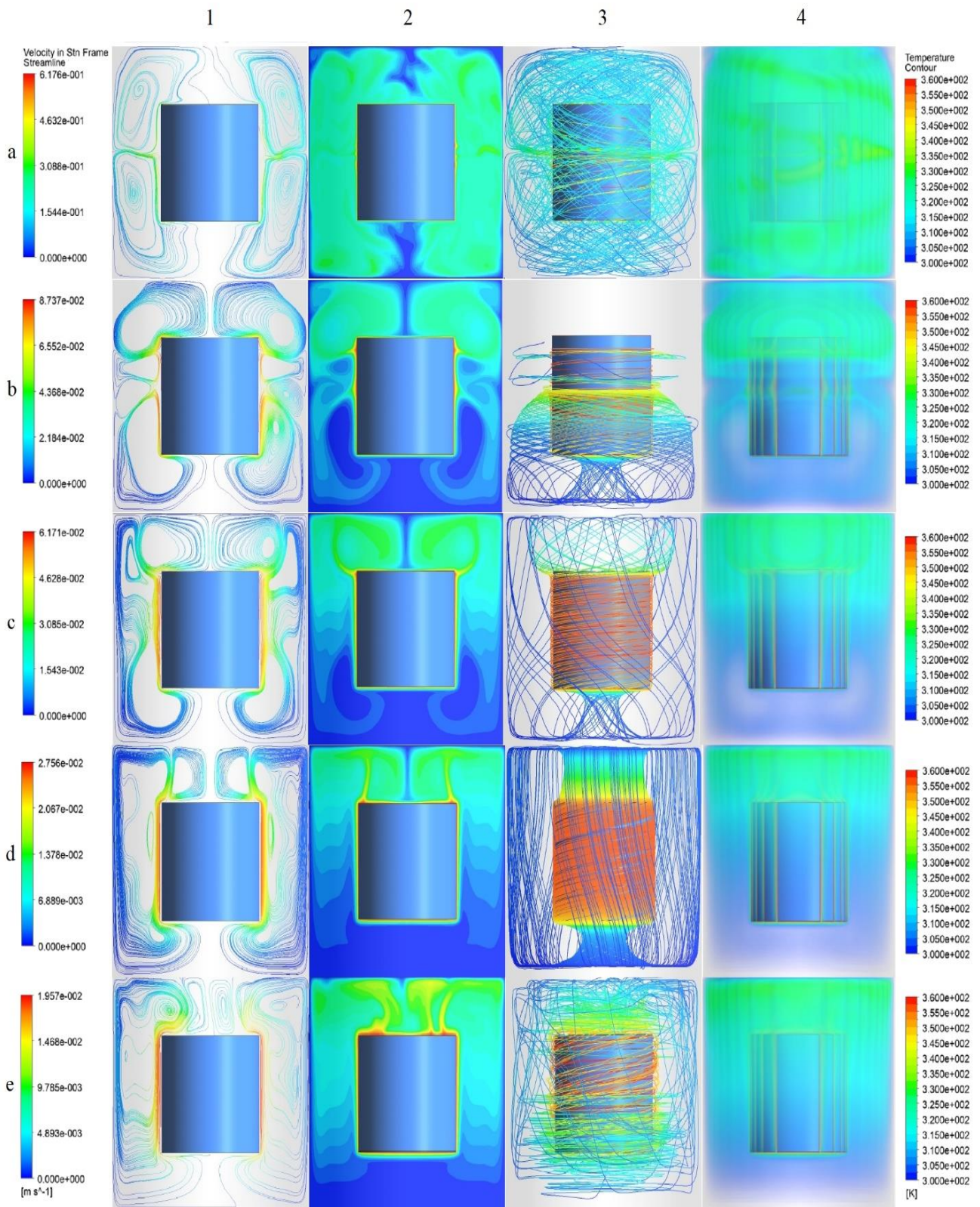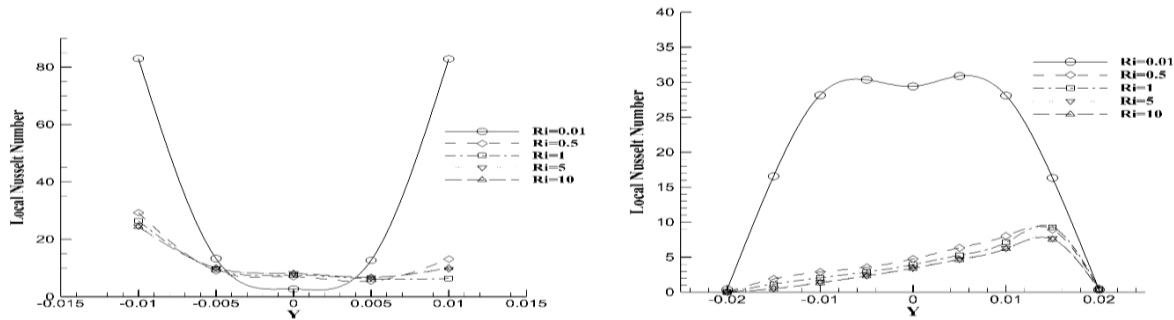
Fig. 11: 2D and 3D streamlines and isotherm contour for different value of Ri at b/a=2 and Pr=55, a(Ri=0.01), b(Ri=0.5), c(Ri=1), d(Ri=5), e(Ri=10)

Table3: comparison between reduction of average nusselt number at different richardson numbers

Pr number	Ri number				
	0.01	0.5	1	5	10
55	-	47.6 %	16.2%	26.8%	23.4%
1205	-	71.2%	20.2%	27.4%	9.5%
5050	-	74.2%	14.9%	24.8%	4.2%

Fig. 12: Comparison of local Nusselt number distribution along the surface for different values of Y and Ri when Pr=5050 and b/a=2: left inner vertical cylinder, right outer enclosure
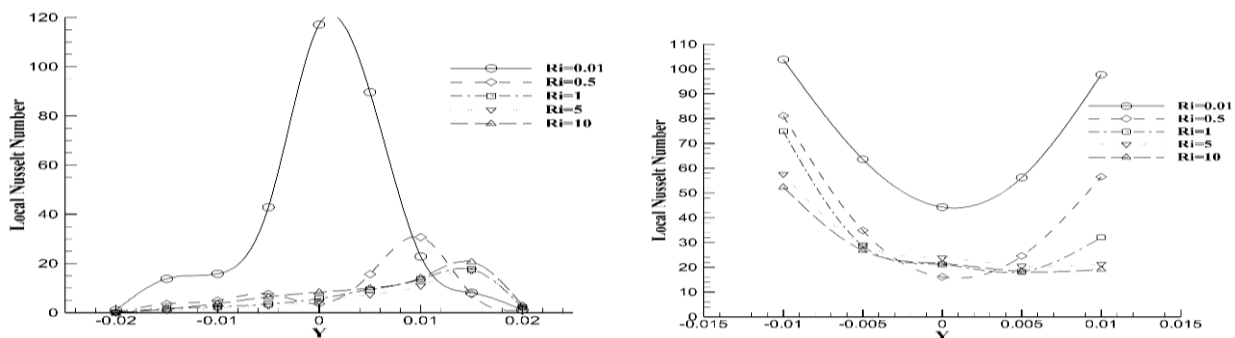
Fig. 13: Comparison of local Nusselt number distribution along the surface for different values of Y and Ri when Pr=55 and b/a=2: left inner vertical cylinder, right outer enclosure
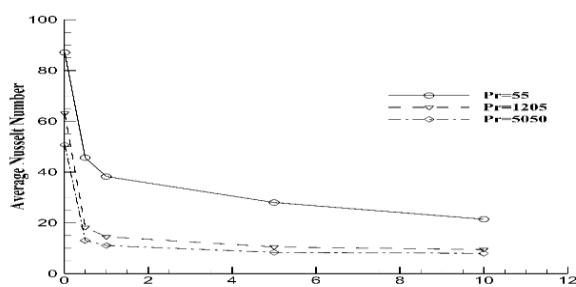
Fig. 14: The relationship between the surface-averaged Nusselt number (Nu$_{Mean}$) and Richardson number (Ri) when b/a=2

3) The effects of Pr on the flow and heat transfer were assessed considering b/a=2 and Pr=55, 1205, and 5050. The isotherm and streamline distributions in the domain have exhibited a strong dependence on Pr, indicating a rise in the thermal boundary layer's thickness over the surface of the inner vertical cylinder with decrementing Pr. The large isotherm region has disappeared by reducing Pr. By reducing the Pr number, many vortices have been formed in the fluid and the problems have become completely unstable. The average Nusselt rate has decreased by reducing the Pr to a constant Ri. As expected, average Nu has decremented by increased Ri for a fixed Pr. By changing the Ri number from 0.01 to 10, the reductions in the averaged Nu have been 75.4%, 84.9%, and 84.2% for Pr=55, 1205, and 5050, respectively.

It seems that the unsteady flow for the rotating vertical cylinder can be studied and investigated the effect of the Pr number, geometry and the Richardson number on the heat transfer phenomenon. Therefore, the future study should be indicated the relationship between the average Nusselt number, the Ri number, and the Pr number on the instability of the flow.

Nomenclature

a	Inner vertical cylinder diameter (m)
b	Outer vertical cylinder diameter (m)
r, θ , z	cylindrical coordinate
s	Height of cylinder (m)
X, Y	Dimensionless cartesian coordinate
V	Velocity (m/s)
T	Temperature (K)
g	Gravitational acceleration (m/s)
h	Heat transfer coefficient (W/m^2/K)
k	Thermal conductivity (W/m/K)
U_0	Reference velocity (m/s)
Pr	Prandtl number
Gr	Grashof number
Ri	Richardson number
Nu_{mean}	Average Nusselt number
Nu_{Local}	Local Nusselt number
Re	Reynolds number

Greek symbol

ν	Kinematic viscosity (m^2/s)
λ	Aspect ratio
w	Angular velocity of cylinder (rad/s)
β	Thermal expansion coefficient (1/K)
$\theta^{..}$	Dimensional Temperature
μ	Dynamic viscosity (N.s/m^2)
ρ	Density (kg/m^3)

Subscript

i	Inner
o	Outer
H	Hot
C	Cold

REFERENCES

[1] Nuttal H., The Slow Rotation of a Circular Cylinder in a Viscous Fluid, *International Journal of Engineering Science*, **2**: 461-476 (1965).

[2] Ostrach S, Natural Convection in Enclosures, *J. Heat Transfer Trans. ASME*, **110**: 1175–1190 (1988).

[3] Hsiao S.W., Chen C.K., Cheng P., A numerical Solution for Natural Convection in an Inclined Porous Cavity with a Discrete Heat Source on a Wall, *International Journal of Heat and Mass Transfer*, **37**: 2193-2201 (1994).

[4] Lei C., Armfield S.W., Patterson J.C., Unsteady Natural Convection in a Waterfilled Isosceles Triangular Enclosure Heated from Below, *International Journal of Heat and Mass Transfer*, **51**: 2637-2650 (2008).

[5] Cho C.C., Chen C.L., Chen C.K., Natural Convection Heat Transfer Performance in Complex-Wavy-Wall Enclosed Cavity Filled with Nanofluid, *International Journal of Thermal Sciences*, **60**: 255-263 (2012).

[6] Kuehn T.H., Goldstein R.J., An Experimental and Theoretical Study of Natural Convection in the Annulus between Horizontal Concentric Cylinders, *Journal of Fluid Mechanics*, **74**: 695 – 719 (1976).

[7] Moukalled F., Acharya S., Natural Convection in the Annulus between Concentric Horizontal Circular and Square Cylinders, *J. Thermophys. Heat Transfer*, **10**: 524–531 (1996).

[8] Hsiao S.W., Cheng P., Chen C.K., Non-Uniform Porosity and Thermal Dispersion Effects on Natural Convection About a Heated Horizontal Cylinder in an Enclosed Porous Medium, *International Journal of Heat and Mass Transfer*, **35**: 3407-3418 (1992).

[9] Shu C., Xue H., Zhu Y.D., Numerical Study of Natural Convection in an Eccentric Annulus between a Square Outer Cylinder and Circular Inner Cylinder Using DQ Method, *International Journal of Heat and Mass Transfer.*, **44**: 3321-3333 (2001).

[10] De A.K., Dalal A., A Numerical Study of Natural Convection Around a Square, Horizontal, Heated Cylinder Placed in an Enclosure, *International Journal of Heat and Mass Transfer*, **49**: 4608-4623 (2006).

[11] Angeli D., Levoni P., Barozzi G., Numerical Predictions for Stable Buoyant Regimes within a Square Cavity Containing a Heated Horizontal Cylinder, *International Journal of Heat and Mass Transfer,* **51**: 553-565 (2008).

[12] Hussain S., Hussein A., Numerical Investigation of Natural Convection Phenomena in a Uniformly Heated Circular Cylinder Immersed in Square Enclosure Filled with Air at Different Vertical Locations, *International Communications in Heat and Mass Transfer*, **37**: 1115-1126 (2010).

[13] Liao C.C., Lin C.A., Influences of a Confined Elliptic Cylinder at Different Aspect Ratios and Inclinations on the Laminar natural and Mixed Convection Flows, *International Journal of Heat and Mass Transfer*, **55**: 6638-6650: (2012).

[14] Cesini G., Paroncini M., Cortella G., Manzan M., Natural Convection from a Horizontal Cylinder in a Rectangular Cavity, *International Journal of Heat and Mass Transfer*, **42**: 1801-1811 (1999).

[15] Corvaro F., Paroncini M., An Experimental Study of Natural Convection in a Differentially Heated Cavity through a 2D-PIV System, *International Journal of Heat and Mass Transfer*, **52:** 355-365, (2009).

[16] Fiscaletti D., Angeli D., Tarozzi L., Barozzi G.S., Buoyancy-Induced Transitional flows Around an Enclosed Horizontal Cylinder, An Experiment, *International Journal of Heat and Mass Transfer*, **58**: 619-631 (2013).

[17] Gupta M.C., Goyal M.C., Viscous Incompressible Flow between Two Coaxial Rotating Circulars with Small Uniform Injection at the Inner Cylinder, *Mathematica*, **2(4)**: (1970).

[18] SMITH S.H., The Rotation of Two Circular Cylinders in a Viscous Fluid, *Mathematica*, **38- 63-66**: (1991).

[19] Hayas T., C.Humphrey J.A., Greif R., Numerical Calculation of Convective Heat Transfer Between Rotating Coaxial Cylinders with Periodically Embedded Cavities, *Journal of Heat Transfer*, **114**: 589-597 (1992).

[20] Kimura T., Takeuchi M., Niroh Nagai, Yoshiaki Kataoka, and Tetsuya Yoshida, Heat Transfer Regulation in a Rectangular Enclosure Using a Rotating Plate, *Heat Transfer—Asian Research*, **32**: 342-353 (2003).

[21] Ding H., Zhu C., Yeo K.S., Lu Z.L., Simulation of Natural Convection in Eccentric Annuli between a Square Outer Cylinder and a Circular Inner Cylinder Using Local MQ-DQ Method, *International Journal of Computation and Methodology*, **47**: 291-313 (2005).

[22] King. M.P., Wilson. M., Numerical Simulation of Convective Heat Transfer in Rayleigh-Bernard Convection and a Rotating Annulus, *Numerical Heat Transfer, Part A*, **48**: 529-545 (2005).

[23] Keh H.J., Wang L.R., Slow Motions of a Circular Cylinder Experiencing Slip Near a Plane Wall, *Journal of Fluids and Structures*, **24**: 651-663 (2008).

[24] Paramane Sachin B., Sharma A., Numerical Investigation of Heat and Fluid Flow Across a Rotating Circular Cylinder Maintained at Constant Temperature in 2-D Laminar Flow Regime, *International Journal of Heat and Mass Transfer*, **52**: 3205-3216 (2009).

[25] Moghadam A., Jabari Baradaran Rahimi A., Similarity Solution in the Study of Flow and Heat Transfer Between Two Rotating Spheres with Constant Angular Velocities, *Scientia Iranica*, **16**: 354-362 (2009).

[26] Costa V.A.F, Raimundo A.M., Steady Mixed Convection in a Differentially Heated Square Enclosure with an Active Rotating Circular Cylinder, *International Journal of Heat and Mass Transfer,* **53**: 1208-1219 (2010).

[27] Salam H.H., Ahmed K.H., Numerical Investigation of Natural Convection Phenomena in a Uniformly Heated Circular Cylinder Immersed in Square Enclosure Filled with Air at Different Vertical Locations, *International Communications in Heat and Mass Transfer*, **37**: 1115-1126 (2010).

[28] Silva A.R.D., Silveira Neto A.D., de Lima A.M.G., Rade D.A., Numerical Simulations of Flows over a Rotating Circular Cylinder Using the Immersed Boundary Method, *J. of the Braz. Soc. of Mech. Sci. & Eng.*, **33**: 99-106, (2011).

[29] Liao C.-C., Lin C.-A., Simulations of Natural and Forced Convection Flows with Moving Embedded Object Using Immersed Boundary Method, *Computer Methods in Applied Mechanics and Engineering*, **213–216**: 58-70 (2012).

[30] Liao C.-C., Lin C.-A., Mixed Convection of a Heated Rotating Cylinder in a Square Enclosure, *International Journal of Heat and Mass Transfer*, **72**: 9-22 (2014).

[31] Ikhtiar U., Manzoor.S, Sheikh N.A., Muzaffar A., Free Stream Flow and Forced Convection Heat Transfer Around a Rotating Circular Cylinder Subjected to a Single Gust Impulse, *International Journal of Heat and Mass Transfer*, **99**: 851-861 (2016).

[32] Hanif R., O.G. B., M. E., S.M., Muzaffar A., N.A. S., Transient Fluid Flow and Heat Transfer over a Rotating Circular Cylinder Near a Wall Subject to a Single Gust Impulse, *International Journal of Heat and Mass Transfer*, **126**: 1178-1193 (2018).

[33] Deepak K., Ramesh K., Chandok S., Mathematical Modeling and Simulation for the Flow of Magneto-Powell-Eyring Fluid in an Annulus with Concentric Rotating Cylinder, *Chinese Journal of Physics*, **65**: 187-197 (2020).

[34] Hatami M., Sun L., Jing D., Günerhan H., Kameswaran Peri K., Rotating Cylinder Turbulator Effect on the Heat Transfer of a Nanofluid Flow in a Wavy Divergent Channel, *Journal of Applied and Computational Mechanics*, **7**: 1987-1998 (2021).

[35] Davoodabadi S., Oztop Hakan F., Natural Convection in a Rectangular Tall Cavity in the Presence of an Oscillating and Rotating Cylinder, *Colloids and Surface A: Physicochemical and Engineering Aspect*, **647**: (2022).

[36] White Frank M., "Fluid Mechanics", 7th Edition, McGraw-Hill, New York (2011).